Articles

Control of Helical Structure in Random Copolymers of Chiral and Achiral Aryl Isocyanides Prepared with Palladium−Platinum μ-Ethynediyl Complexes

Fumie Takei, Kiyotaka Onitsuka,* and Shigetoshi Takahashi

The Institute of Scientific and Industrial Research, Osaka University, 8-1 Mihogaoka, Ibaraki, Osaka 567-0047, Japan

Ken Terao and Takahiro Sato*

Department of Macromolecular Science, Osaka University, 1-1 Machikaneyama-cho, Toyonaka, Osaka 560-0043, Japan

Received April 16, 2007; Revised Manuscript Received May 12, 2007

ABSTRACT: Random copolymerization of aryl isocyanides possessing chiral and achiral alkoxycarbonyl groups at *p*- or *m*-positions was initiated with the Pd−Pt μ-ethynediyl complex to give in good yields the corresponding polymers with narrow polydispersity indexes. The selective formation of the one-handed helical structure in the resulting polymers was confirmed by the large values of specific rotation and the CD spectra showing the Cotton effect around 364 nm. The helical sense selectivity was strongly dependent on not only the contents of chiral monomers but also the structures of chiral and achiral monomers. Notably, inversion of helical sense was observed in random copolymers prepared from *m*-substituted chiral and *p*-substituted achiral aryl isocyanides depending on the content of the monomers. Those results were compared with a novel theory of the helical sense selective polymerization kinetics, which explained both strong dependence of the helical sense selectivity and weak dependence of the propagation reaction rate on the chiral monomer content.

Introduction

Artificial polymers that possess the one-handed helical structure have recently attracted considerable interest due to their potential as a new advanced material having molecular recognition ability and asymmetric catalysis as well as biomimetic functions.[1] Artificial helical polymers usually consist of two conformational stereoisomers with right-handed (*P*) and left-handed (*M*) helices. As the introduction of chiral pendants into helical polymers causes *P* and *M* helices to become diastereomers and no longer equivalent, one-handed helical polymers are predominantly produced by the appropriate choice of chiral pendants. Green et al. reported that a small amount of chiral bias determines the helical sense of polyisocyanate,[2] and similar phenomena were observed in polyacetylene.[3] The helical conformation of these polymers is dynamic, and allowed to change its enantiomer excess with temperature in solution.[4] On the other hand, polyisocyanides and polymethacrylates possessing bulky substituents is a representative example of artificial helical polymers exhibiting static nonequilibrium helical conformation even in solution.[1,5] Nolte et al. reported the optical resolution of right- and left-handed helical polyisocyanides with achiral bulky side chain, using a chiral column chromatography, which demonstrates that the helical conformation of polyisocyanide is not interconvertible.[6] Nolte et al. also reported that the random copolymerization of chiral and achiral isocyanides led to the selective formation of one-handed helical polyisocyanides using a Ni initiator, and ascribed the selectivity to the difference in the propagation rate between the chiral and achiral monomers.[7]

Previously, we found that the Pd−Pt μ-ethynediyl complex (**1**) is effective for the living polymerization of aryl isocyanides to give narrow molecular weight distributions.[8] We have succeeded to apply this living polymerization system to the selective synthesis of polyisocyanides with the preferential one-handed helical structure from achiral bulky monomers.[9] However, a chiral living oligomer complex polymerized isocyanide enantiomers with almost the same reaction rate constant, implying that the helical sense of polyisocyanides would not be explained kinetically as done by Nolte et al. The difference from Nolte et al. 's system prompted us to investigate the random copolymerization of chiral and achiral isocyanides with **1**. We report herein the control of helical sense in random copolymers formed with some combinations of chiral and achiral isocyanides, and propose a kinetic theory to explain the screw-sense-sensitive copolymerization. The preliminary results have been reported elsewhere.[10]

Results

Treatment of 50 equiv of *p*-(1*R*,2*S*,5*R*)-menthyloxycarbonylphenyl isocyanide (**2a**) and 50 equiv of *p*-cyclohexyloxycarbonylphenyl isocyanide (**3a**) with complex **1** in refluxing THF for 15 h produced copolymer poly-*r*-**2a**$_{50}$**3a**$_{50}$ ($n = 50$, $m = 50$, $M_w = 14{,}200$, $M_w/M_n = 1.14$) quantitatively (Scheme 1). Since both isocyanide monomers were completely consumed, the

10.1021/ma070891w CCC: $37.00
Published on Web 06/28/2007

Table 1. Copolymerization of *p*-Substituted Chiral and Achiral Isocyanides (2 and 3) with 1

entry	Ar*NC	*n*	ArNC	*m*	polymer	$M_n \times 10^{-3}$ [a]	M_w/M_n	$[\alpha]_D^{20}$ [b]	$\Delta\epsilon_{364}$,[c] dm^3 cm^{-1} mol^{-1}
1			**3a**	100	poly-**3a**$_{100}$	13.3	1.13	0	0
2	**2a**	30	**3a**	70	poly-*r*-**2a**$_{30}$**3a**$_{70}$	12.0	1.15	582	5.12
3	**2a**	50	**3a**	50	poly-*r*-**2a**$_{50}$**3a**$_{50}$	12.5	1.14	890	9.40
4	**2a**	70	**3a**	30	poly-*r*-**2a**$_{70}$**3a**$_{30}$	12.5	1.12	1054	11.58
5	**2a**	100			poly-**2a**$_{100}$	12.9	1.12	1079	13.01
6			**3b**	100	poly-**3b**$_{100}$	*d*	*d*	*d*	*d*
7	**2a**	30	**3b**	70	poly-*r*-**2a**$_{30}$**3b**$_{70}$	12.9	1.13	565	4.51
8	**2a**	50	**3b**	50	poly-*r*-**2a**$_{50}$**3b**$_{50}$	13.1	1.12	855	7.55
9	**2a**	70	**3b**	30	poly-*r*-**2a**$_{70}$**3b**$_{30}$	12.9	1.11	1083	10.13
10	**2b**	30	**3a**	70	poly-*r*-**2b**$_{30}$**3a**$_{70}$	12.6	1.13	−552	−5.92
11	**2b**	50	**3a**	50	poly-*r*-**2b**$_{50}$**3a**$_{50}$	12.7	1.13	−909	−9.07
12	**2b**	70	**3a**	30	poly-*r*-**2b**$_{70}$**3a**$_{30}$	12.0	1.15	−1014	−12.24
13	**2b**	100			poly-**2b**$_{100}$	13.4	1.12	−1054	−12.59
14	**2a**	30	**3a**	70	poly-*b*-**2a**$_{30}$**3a**$_{70}$	13.0	1.15	393	3.46
15	**2a**	50	**3a**	50	poly-*b*-**2a**$_{50}$**3a**$_{50}$	12.7	1.13	599	6.70
16	**2a**	70	**3a**	30	poly-*b*-**2a**$_{70}$**3a**$_{30}$	12.9	1.13	832	9.86
17	**2a**	30	**3b**	70	poly-*b*-**2a**$_{30}$**3b**$_{70}$	13.1	1.15	441	3.58
18	**2a**	50	**3b**	50	poly-*b*-**2a**$_{50}$**3b**$_{50}$	13.0	1.14	685	5.95
19	**2a**	70	**3b**	30	poly-*b*-**2a**$_{70}$**3b**$_{30}$	13.6	1.12	885	8.29
20	**2b**	30	**3a**	70	poly-*b*-**2b**$_{30}$**3a**$_{70}$	12.8	1.12	−393	−3.65
21	**2b**	50	**3a**	50	poly-*b*-**2b**$_{50}$**3a**$_{50}$	13.1	1.12	−629	−5.93
22	**2b**	70	**3a**	30	poly-*b*-**2b**$_{70}$**3a**$_{30}$	13.6	1.12	−878	−9.28

[a] By GPC analyses using polystyrene standard. [b] $CHCl_3$, *c* 0.1. [c] CD spectra were measured in $CHCl_3$ at ambient temperature. The $\Delta\epsilon$ values are based on the average molecular mass of an isocyanide monomer unit. [d] Molecular weight and specific rotation could not be measured due to low solubility.

Scheme 1

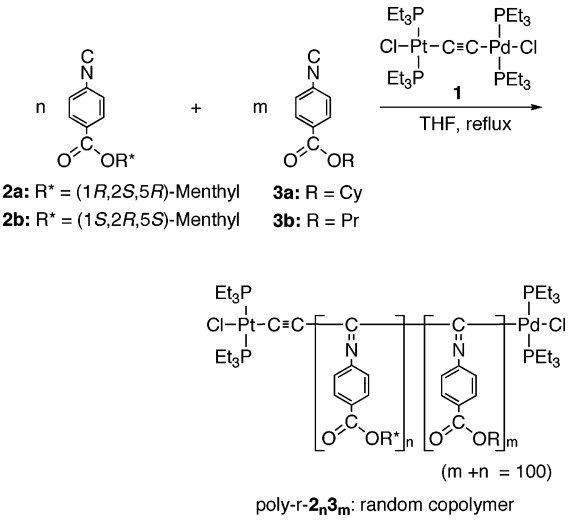

composition of **2a** and **3a** in the resulting polymer should be 1:1, which was supported by elemental analysis. When the copolymerization was stopped at approximately 60% conversion, the ratio of unreacted **2a** to **3a** was 1:1.2, which was consistent with the small difference in the homopolymerization rate (**2a**, $k = 2.60 \times 10^{-5}$ s^{-1}; **3a**, $k = 1.99 \times 10^{-5}$ s^{-1}, 338 K, $[1]_0 =$ 0.50 mM, $[\text{monomer}]_0 = 25.0$ mM). These results suggested that poly-*r*-**2a**$_{50}$**3a**$_{50}$ is a random copolymer, as expected.

In the CD spectrum of poly-*r*-**2a**$_{50}$**3a**$_{50}$, a strong Cotton effect was observed at 364 nm, which is characteristic of helical chiral poly(aryl isocyanide)s (Figure 1), and the molar circular dichroism at 364 nm ($\Delta\epsilon_{364}$) of poly-*r*-**2a**$_{50}$**3a**$_{50}$ was slightly smaller than that of homopolymer poly-**2a**$_{100}$ (Chart 1). No significant change was observed in the CD spectra of poly-*r*-**2a**$_{50}$**3a**$_{50}$ in the range of −70 °C to 50 °C in $CHCl_3$, as observed in poly-**2a**$_{100}$. Poly-*r*-**2a**$_{50}$**3a**$_{50}$ showed a large positive specific rotation $[\alpha]^{20}_D = +890$, whereas the $[\alpha]^{20}_D$ value of poly-**2a**$_{100}$ was even larger at +1079. These data clearly showed that poly-*r*-**2a**$_{50}$**3a**$_{50}$ maintained predominantly a one-handed helical structure with the same screw sense as that of poly-**2a**$_{100}$ in solution.[9c] The positive $\Delta\epsilon_{364}$ value suggested that poly-*r*-**2a**$_{50}$**3a**$_{50}$ preferred a right-handed helix.[9e] However, the helical

Scheme 2

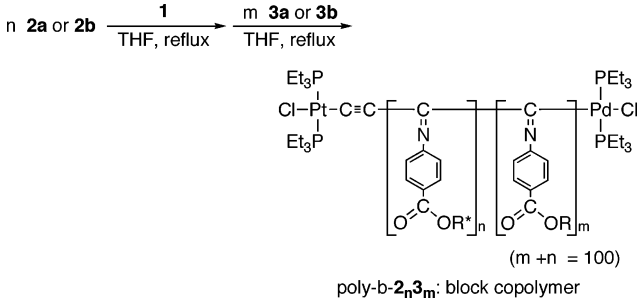

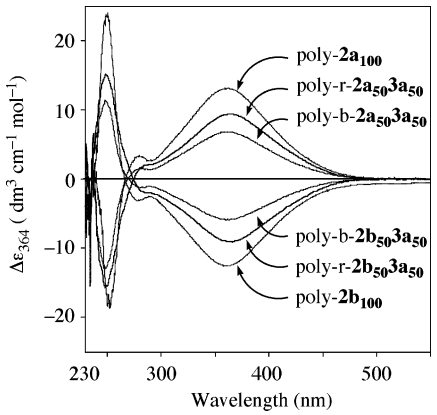

Figure 1. CD spectra of random and block copolymers poly-*r*-**2a**$_{50}$**3a**$_{50}$, poly-*b*-**2a**$_{50}$**3a**$_{50}$, poly-*r*-**2b**$_{50}$**3a**$_{50}$, and poly-*b*-**2b**$_{50}$**3a**$_{50}$, and chiral homopolymers poly-**2a**$_{100}$ and poly-**2b**$_{100}$.

Chart 1

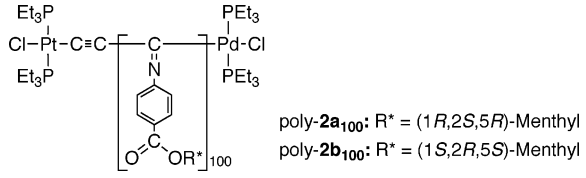

sense selectivity of poly-*r*-**2a**$_{50}$**3a**$_{50}$ was slightly lower than that of poly-**2a**$_{100}$. This result sharply contrasted the fact that the copolymer of chiral and achiral isocyanides with Ni catalyst keeps predominantly a one-handed helical structure,

Scheme 3

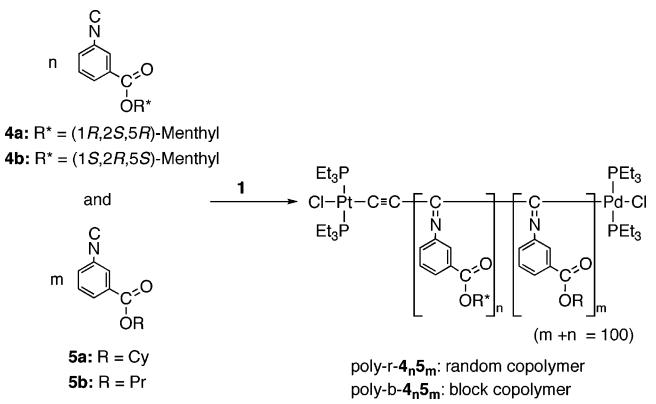

the helical sense of which is opposite that of the homopolymer prepared from the chiral isocyanide.[7] It may be of interest that the achiral isocyanide monomer **3a** was not bulky enough to maintain the helical structure of the homopolymer formed from it.[9c]

Random copolymerization involving the combination of **2a** and *p*-(1*R*,2*S*,5*R*)-menthyloxycarbonylphenyl isocyanide (**2b**) with **3a** and *p*-propoxycarbonylphenyl isocyanide (**3b**) at several molar ratios was performed while controlling the feed ratio of **1**/monomers at 1/100. All polymerizations proceeded smoothly and random copolymers poly-*r*-**2**$_n$**3**$_m$, the molecular weights of which were essentially the same, were obtained in quantitative yields. Thus, the contents of **2** and **3** in the resulting polymers poly-*r*-**2**$_n$**3**$_m$ were equal to the initial ratio of the monomers. Block copolymers (poly-*b*-**2**$_n$**3**$_m$) with the same monomer ratio were also prepared by successive reactions of **2** and **3** with **1** (Scheme 2).[9c] The results are summarized in Table 1. Some copolymers were prepared multiple times, and the errors of molecular weight and chiroptical data were approximately less than 10%. The helical sense selectivity of the resulting copolymers poly-*r*-**2**$_n$**3**$_m$ and poly-*b*-**2**$_n$**3**$_m$ was estimated by comparing their $\Delta\epsilon_{364}$ values. Figure 2 shows plots of the $\Delta\epsilon_{364}$ values of poly-*r*-**2**$_n$**3**$_m$ as well as poly-*b*-**2**$_n$**3**$_m$ as a function of chiral monomer content. In poly-*b*-**2**$_n$**3**$_m$, the polymer block composed of **2a** and **2b** maintains predominantly a one-handed helix, whereas the polymer block composed of achiral isocyanides **3a** and **3b** does not keep a helical structure.[9c] Therefore, the $\Delta\epsilon_{364}$ values of poly-*b*-**2**$_n$**3**$_m$ are almost proportionally increased with an increase in the chiral monomer content. In contrast, the $\Delta\epsilon_{364}$ values of poly-*r*-**2**$_n$**3**$_m$ are larger than those of the corresponding block copolymers poly-*b*-**2**$_n$**3**$_m$, and a positive nonlinear relationship is observed in all cases. Typically, the Cotton effect at 364 nm of random copolymers poly-*r*-**2a**$_{70}$**3a**$_{30}$, poly-*r*-**2b**$_{70}$**3a**$_{30}$ and poly-*r*-**2a**$_{70}$**3b**$_{30}$ is as large as that of chiral homopolymers poly-**2a**$_{100}$ and poly-**2b**$_{100}$. Similar phenomena were found in the specific rotation of the polymers.

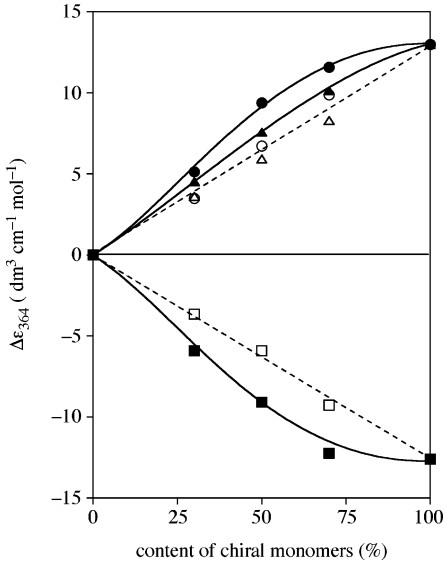

Figure 2. Plots of molar circular dichroism vs content of chiral monomers **2a** and **2b** in random copolymers poly-*r*-**2a**$_n$**3a**$_m$ (●), poly-*r*-**2a**$_n$**3b**$_m$ (▲), and poly-*r*-**2b**$_n$**3a**$_m$ (■) and block copolymers poly-*b*-**2a**$_n$**3a**$_m$ (○), poly-*b*-**2a**$_n$**3b**$_m$ (△), and poly-*b*-**2b**$_n$**3a**$_m$ (□).

The random and block copolymerization of chiral and achiral *m*-substituted aryl isocyanides (**4** and **5**) gave copolymers poly-*r*-**4**$_n$**5**$_m$ and poly-*b*-**4**$_n$**5**$_m$ in quantitative yields (Scheme 3). The results are summarized in Table 2. The Cotton effect at 364 nm suggested that poly-*r*-**4**$_n$**5**$_m$ formed predominantly helical structures, the senses of which were the same as those of homopolymer poly-**4**$_n$. The $\Delta\epsilon_{364}$ values of poly-*r*-**4**$_n$**5**$_m$ and poly-*b*-**4**$_n$**5**$_m$ are plotted against the ratio of chiral monomers

Table 2. Copolymerization of *m*-Substituted Chiral and Achiral Isocyanides (4 and 5) with 1

entry	Ar*NC	*n*	ArNC	*m*	polymer	$M_n \times 10^{-3}$ [a]	M_w/M_n	$[\alpha]_D^{20}$ [b]	$\Delta\epsilon_{364}$,[c] dm^3 cm^{-1} mol^{-1}
1			**5a**	100	poly-**5a**$_{100}$	12.2	1.06	0	0
2	**4a**	30	**5a**	70	poly-*r*-**4a**$_{30}$**5a**$_{70}$	12.6	1.08	75	0.94
3	**4a**	50	**5a**	50	poly-*r*-**4a**$_{50}$**5a**$_{50}$	13.3	1.08	156	1.73
4	**4a**	70	**5a**	30	poly-*r*-**4a**$_{70}$**5a**$_{30}$	13.0	1.07	179	2.20
5	**4a**	100			poly-**4a**$_{100}$	13.0	1.06	270	2.81
6			**5b**	100	poly-**5b**$_{100}$	12.6	1.03	0	0
7	**4a**	30	**5b**	70	poly-*r*-**4a**$_{30}$**5b**$_{70}$	13.3	1.07	52	0.58
8	**4a**	50	**5b**	50	polyr-**4a**$_{50}$**5b**$_{50}$	13.4	1.07	116	1.35
9	**4a**	70	**5b**	30	poly-*r*-**4a**$_{70}$**5b**$_{30}$	13.7	1.06	159	1.79
10	**4b**	30	**5a**	70	poly-*r*-**4b**$_{30}$**5a**$_{70}$	13.8	1.06	−108	−1.11
11	**4b**	50	**5a**	50	poly-*r*-**4b**$_{50}$**5a**$_{50}$	13.8	1.06	−153	−1.69
12	**4b**	70	**5a**	30	poly-*r*-**4b**$_{70}$**5a**$_{30}$	13.8	1.06	−195	−2.18
13	**4b**	100			poly-**4b**$_{100}$	12.8	1.09	−260	−2.89
14	**4a**	30	**5a**	70	poly-*b*-**4a**$_{30}$**5a**$_{70}$	13.7	1.07	96	0.87
15	**4a**	50	**5a**	50	poly-*b*-**4a**$_{50}$**5a**$_{50}$	13.7	1.08	213	2.00
16	**4a**	70	**5a**	30	poly-*b*-**4a**$_{70}$**5a**$_{30}$	13.4	1.07	246	2.61
17	**4a**	30	**5b**	70	poly-*b*-**4a**$_{30}$**5b**$_{70}$	13.9	1.07	129	1.12
18	**4a**	50	**5b**	50	poly-*b*-**4a**$_{50}$**5b**$_{50}$	13.7	1.08	200	1.65
19	**4a**	70	**5b**	30	poly-*b*-**4a**$_{70}$**5b**$_{30}$	13.7	1.07	246	2.56
20	**4b**	30	**5a**	70	poly-*b*-**4b**$_{30}$**5a**$_{70}$	13.5	1.06	−138	−1.13
21	**4b**	50	**5a**	50	poly-*b*-**4b**$_{50}$**5a**$_{50}$	13.3	1.06	−209	−1.94
22	**4b**	70	**5a**	30	poly-*b*-**4b**$_{70}$**5a**$_{30}$	13.7	1.06	−264	−2.83

[a] By GPC analyses using polystyrene standard. [b] $CHCl_3$, *c* 0.1. [c] CD spectra were measured in $CHCl_3$ at ambient temperature. The $\Delta\epsilon$ values are based on the average molecular mass of an isocyanide monomer unit.

Chart 2

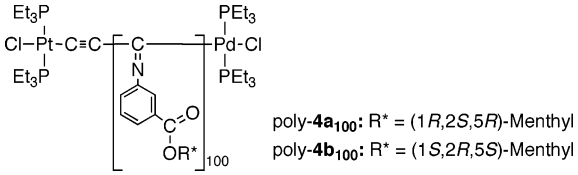

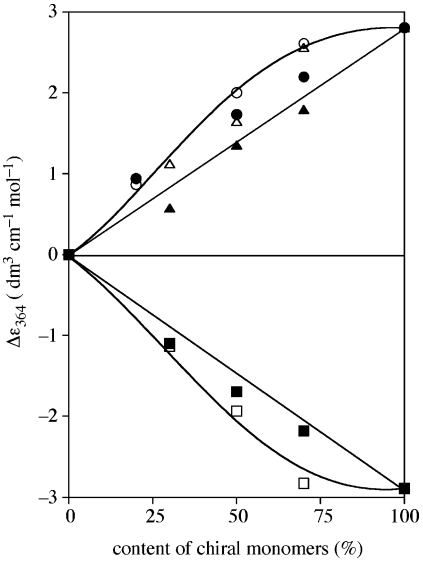

Figure 3. Plots of molar circular dichroism vs content of chiral monomers **4a** and **4b** in random copolymers poly-*r*-**4a**$_n$**5a**$_m$ (●), poly-*r*-**4a**$_n$**5b**$_m$ (▲), and poly-*r*-**4b**$_n$**5a**$_m$ (■) and block copolymers poly-*b*-**4a**$_n$**5a**$_m$ (○), poly-*b*-**4a**$_n$**5b**$_m$ (△), and poly-*b*-**4b**$_n$**5a**$_m$ (□).

Scheme 4

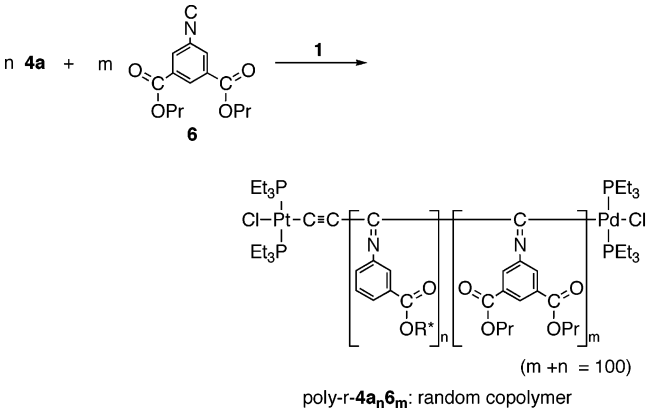

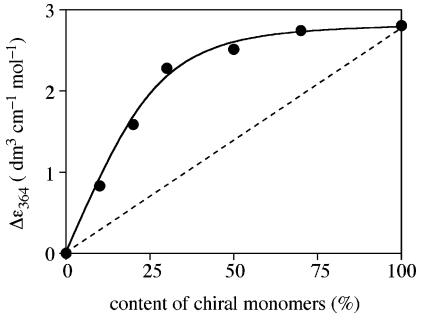

Figure 4. Plots of molar circular dichroism vs content of chiral monomer **4a** in random copolymer poly-*r*-**4a**$_n$**6**$_m$.

4a and **4b** to achiral monomers **5a** and **5b** in Figure 3. In contrast to the results of *p*-substituted copolymers shown in Figure 2, the $\Delta\epsilon_{364}$ values of poly-*r*-**4**$_n$**5**$_m$ are increased almost proportionally with an increase of the chiral monomer content, while a positive nonlinear relationship is noted in poly-*b*-**4**$_n$**5**$_m$, suggesting that the connecting part of the homopolymer block formed from **5** with the one handed helical homopolymer block formed from **4** follows the helical structure, whereas the other part has a random structure.

We have experimental evidence that 3,5-disubstituted aryl isocyanide is bulky enough for its homopolymer to keep the helical structure.[9a,c] Thus, we also performed random copolymerization of **4a** and 3,5-di(propoxycarbonyl)aryl isocyanide (**6**) to give poly-*r*-**4a**$_n$**6**$_m$ (Scheme 4). As expected, poly-*r*-**4a**$_n$**6**$_m$ showed strong Cotton effect and a large specific rotation compared with poly-*r*-**4a**$_n$**5a**$_m$ at the same content of **4a** (Table 3). As seen in Figure 4, the $\Delta\epsilon_{364}$ values are not proportional to the content of **4a**, showing marked convex deviation from linearity.

When chiral monomers were copolymerized with achiral monomers having alkoxycarbonyl groups at different positions on the aromatic ring from that of chiral ones, interesting results were obtained (Scheme 5 and Tables 4 and 5). Poly-*r*-**2a**$_{50}$**5a**$_{50}$ showed very weak Cotton effect and small specific rotation compared with poly-**2a**$_{100}$. The $\Delta\epsilon_{364}$ values of poly-*r*-**2a**$_n$**5a**$_m$ plotted against chiral monomer contents in Figure 5 showed marked negative nonlinearity.

To our surprise, poly-*r*-**4a**$_{50}$**3a**$_{50}$ showed negative Cotton effect at 364 nm and negative specific rotation, whereas poly-**4a**$_{100}$ exhibited positive Cotton effect and positive specific rotation. These results clearly suggested that poly-*r*-**4a**$_{50}$**3a**$_{50}$ formed predominantly a left-handed helical structure opposite that of poly-**4a**$_{100}$. As seen in Figure 6, the magnitude of the

Table 3. Random Copolymerization of *m*-Substituted Chiral and 3,5-Disubstituted Achiral Isocyanides (4a and 6) with 1

entry	*n* (**4a**)	*m* (**6**)	polymer	$M_n \times 10^{-3}$ [a]	M_w/M_n	$[\alpha]_D^{20}$ [b]	$\Delta\epsilon_{364}$,[c] dm^3 cm^{-1} mol^{-1}
1	10	90	poly-*r*-**4a**$_{10}$**6**$_{90}$	13.7	1.10	113	0.83
2	20	80	poly-*r*-**4a**$_{20}$**6**$_{80}$	13.8	1.09	182	1.59
3	30	70	poly-*r*-**4a**$_{30}$**6**$_{70}$	12.0	1.08	230	2.28
4	50	50	poly-*r*-**4a**$_{50}$**6**$_{50}$	12.7	1.07	264	2.51
5	70	30	poly-*r*-**4a**$_{70}$**6**$_{30}$	12.7	1.07	278	2.74

[a] By GPC analyses using polystyrene standard. [b] $CHCl_3$, *c* 0.1. [c] CD spectra were measured in $CHCl_3$ at ambient temperature. The $\Delta\epsilon$ values are based on the average molecular mass of an isocyanide monomer unit.

Table 4. Random Copolymerization of *p*-Substituted Chiral and *m*-Substituted Achiral Isocyanides (2a and 5a) with 1

entry	*n* (**2a**)	*m* (**5a**)	polymer	$M_n \times 10^{-3}$ [a]	M_w/M_n	$[\alpha]_D^{20}$ [b]	$\Delta\epsilon_{364}$,[c] dm^3 cm^{-1} mol^{-1}
1	30	70	poly-*r*-**2a**$_{30}$**5a**$_{70}$	13.3	1.09	14	0.35
2	50	50	poly-*r*-**2a**$_{50}$**5a**$_{50}$	13.8	1.09	149	1.37
3	70	30	poly-*r*-**2a**$_{70}$**5a**$_{30}$	14.3	1.12	532	6.35

[a] By GPC analyses using polystyrene standard. [b] $CHCl_3$, *c* 0.1. [c] CD spectra were measured in $CHCl_3$ at ambient temperature. The $\Delta\epsilon$ values are based on the average molecular mass of an isocyanide monomer unit.

Table 5. Random Copolymerization of *m*-Substituted Chiral and *p*-Substituted Achiral Isocyanides (4a and 3a) with 1

entry	*n* (**4a**)	*m* (**3a**)	polymer	$M_n \times 10^{-3}$ [a]	M_w/M_n	$[\alpha]_D^{20}$ [b]	$\Delta\epsilon_{364}$,[c] dm^3 cm^{-1} mol^{-1}
1	10	90	poly-*r*-**4a$_{10}$3a$_{90}$**	12.6	1.08	−113	−0.58
2	20	80	poly-*r*-**4a$_{20}$3a$_{80}$**	13.1	1.08	−161	−1.20
3	30	70	poly-*r*-**4a$_{30}$3a$_{70}$**	12.1	1.08	−224	−1.66
4	40	60	poly-*r*-**4a$_{40}$3a$_{60}$**	13.1	1.10	−235	−1.76
5	50	50	poly-*r*-**4a$_{50}$3a$_{50}$**	13.0	1.08	−212	−1.54
6	70	30	poly-*r*-**4a$_{70}$3a$_{30}$**	12.6	1.08	−132	−0.79
7	80	20	poly-*r*-**4a$_{80}$3a$_{20}$**	14.2	1.10	−56	0.13
8	85	15	poly-*r*-**4a$_{85}$3a$_{15}$**	13.8	1.08	4	0.58
9	90	10	poly-*r*-**4a$_{90}$3a$_{10}$**	13.5	1.08	63	1.10

[a] By GPC analyses using polystyrene standard. [b] $CHCl_3$, *c* 0.1. [c] CD spectra were measured in $CHCl_3$ at ambient temperature. The $\Delta\epsilon$ values are based on the average molecular mass of an isocyanide monomer unit.

Table 6. Random Copolymerization of *p*- and *m*-Substituted Chiral Isocyanides (2a and 4a) with 1

entry	*n* (**2a**)	*m* (**4a**)	polymer	$M_n \times 10^{-3}$ [a]	M_w/M_n	$[\alpha]_D^{20}$ [b]	$\Delta\epsilon_{364}$,[c] dm^3 cm^{-1} mol^{-1}
1	30	70	poly-*r*-**2a$_{30}$4a$_{70}$**	13.4	1.13	−108	−0.05
2	50	50	poly-*r*-**2a$_{50}$4a$_{50}$**	13.7	1.10	−78	0.43
3	70	30	poly-*r*-**2a$_{70}$4a$_{30}$**	14.0	1.11	274	3.48

[a] By GPC analyses using polystyrene standard. [b] $CHCl_3$, *c* 0.1. [c] CD spectra were measured in $CHCl_3$ at ambient temperature. The $\Delta\epsilon$ values are based on the molecular mass of an isocyanide monomer unit.

Scheme 5

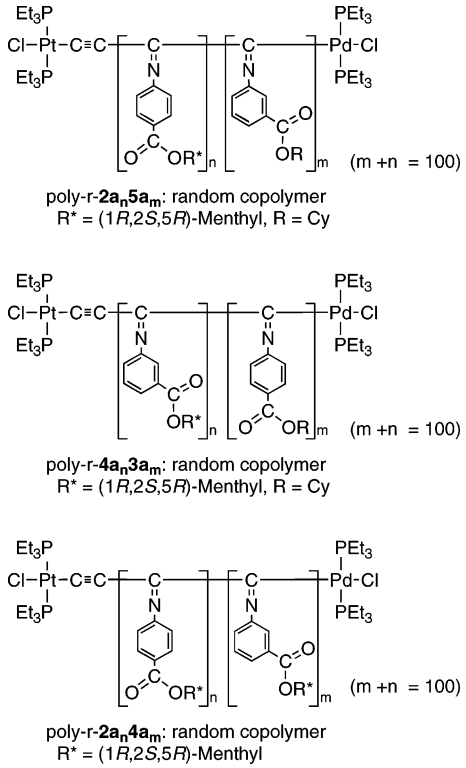

$\Delta\epsilon_{364}$ value with a negative sign is increased with an increase of the chiral monomer content up to 40 mol %, and is decreased in the region up to 80 mol %. Poly-*r*-**4a$_{90}$3a$_{10}$** had a helical structure with the same helical sense as poly-*r*-**4a$_{100}$**, although the selectivity of the helical conformation was still low. This is the second example of the helix sense inversion by copolymerization of chiral and achiral isocyanides. The first one found by Nolte et al. was however the combination of chiral and achiral monomers with very much different propagation rate constants, i.e., it may not be a random copolymerization.[7] On the other hand, our copolymers had narrow molecular weight distributions and the copolymerization should be random. Therefore, we should interpret the helical sense inversion of the copolymer in a different manner from Nolte et al.'s interpretation.

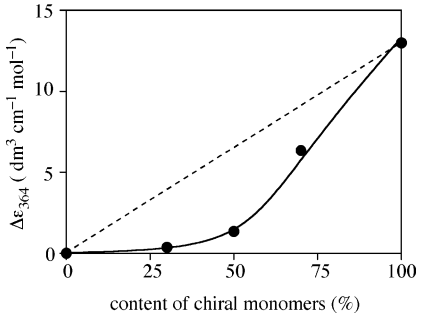

Figure 5. Plots of molar circular dichroism vs content of chiral monomer **2a** in random copolymer poly-*r*-**2a$_n$5a$_m$**.

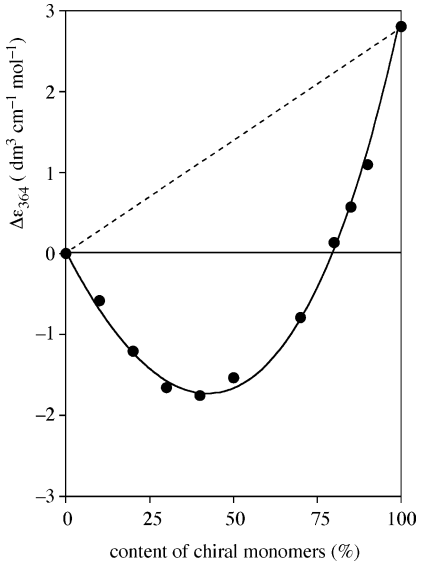

Figure 6. Plots of molar circular dichroism vs content of chiral monomer **4a** in random copolymer poly-*r*-**4a$_n$3a$_m$**.

Helix sense inversions by the chiral-achiral copolymerization have been also reported in polysilylene,[11,12] polyacetylene,[13] and polyisocyanate.[14] However, the main-chain helical conformations of those polymers are dynamical to allow the helix−helix inversion of each monomer unit, and the statistical mechanical argument using the Ising model can be applied to explain their helix sense inversion, being different from our copolyisocyanides

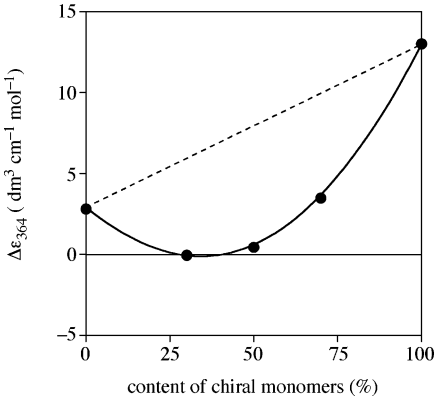

Figure 7. Plots of molar circular dichroism vs content of chiral monomer **2a** in random copolymer poly-*r*-**2a**$_n$**4a**$_m$.

with a nondynamical main chain.

Peculiar helical sense selectivity was also observed in the random copolymer of two chiral monomers (Table 6), the homopolymers of which maintained the same helical sense. Poly-*r*-**2a$_{50}$4a$_{50}$** prepared from the copolymerization of **2a** and **4a** hardly showed the Cotton effect at 364 nm, suggesting that the one-handed helix is not formed predominantly.[9e] This result sharply contrasts the fact that both poly-**2a$_{100}$** and poly-**4a$_{100}$** have predominantly a right-handed helix. Poly-*r*-**2a$_{30}$4a$_{70}$** does not also have the one-handed helical structure, whereas poly-*r*-**2a$_{70}$4a$_{30}$** preferred a right-handed helix with low selectivity. The plots of the $\Delta\epsilon_{364}$ values against the monomer contents exhibited marked negative nonlinearity (Figure 7).

Discussion

Propagation Reaction Kinetics. During the copolymerization of helix-forming chiral and achiral monomers, there are four different types of the reactive end: the chiral monomer unit taking the right-handed helical state ($\cdots P_C$) and left-handed helical state ($\cdots M_C$) as well as the achiral monomer unit taking the right-handed helical state ($\cdots P_A$) and left-handed helical state ($\cdots M_A$). In the propagation reaction, each reactive end may react with chiral or achiral monomer (Mon_C or Mon_A), and the following different types of the propagation reaction can take place:

$$\begin{cases} \cdots P_\alpha + Mon_\beta \xrightarrow{k_{P,\alpha\beta}} \cdots P_\beta & k_{P,\alpha\beta} = k_{AA}\exp(-\Delta G_{h,\alpha\beta}{}^\dagger/RT) \\ \cdots M_\alpha + Mon_\beta \xrightarrow{k_{M,\alpha\beta}} \cdots M_\beta & k_{M,\alpha\beta} = k_{AA}\exp(\Delta G_{h,\alpha\beta}{}^\dagger/RT) \\ \cdots P_\alpha + Mon_\beta \xrightarrow{k_{r,\alpha\beta}} \cdots P_\beta & k_{r,\alpha\beta} = k_{AA}\exp(-\Delta G_{r,\alpha\beta}{}^\dagger/RT) \\ \cdots M_\alpha + Mon_\beta \xrightarrow{k_{r,\alpha\beta}} \cdots P_\beta & \end{cases} \quad (1)$$

where the subscripts α and β indicate the type of monomer or monomer unit (C or A). The rate constants of the propagation reactions, $k_{P,\alpha\beta}$, $k_{M,\alpha\beta}$, and k_r, may be written in the right-hand side forms according to the transition-state theory for the reaction rate. In the equations for the rate constants, k_{AA} is the rate constant of the achiral monomer, $2\Delta G_{h,\alpha\beta}{}^\dagger$ is the difference in the activation free energy (per mole of reaction) between the PP and MM sequence formations by monomer units α and β ($\Delta G_{h,AA}{}^\dagger = 0$), $\Delta G_{r,\alpha\beta}{}^\dagger$ is the excess activation free energy of the helix reversal reaction between monomers α and β, and RT is the gas constant multiplied by the absolute temperature.

If the helical state of the polymer chain does not change after polymerization, it is determined in the polymerization process. Since the rate constants $k_{P,\alpha\beta}$, $k_{M,\alpha\beta}$, and $k_{r,\alpha\beta}$ are proportional to probabilities that the $\alpha\beta$ sequences take the P helical, M helical, and helix reversal states, respectively, during the propagation reaction, we can calculate the average numbers of monomer units taking those helical states using the Ising model theory where the statistical weights of appearance of the corresponding helical states on the sequences are replaced by those rate constants. Since the relation between the rate constant and activation free energy is identical with the relation between the statistical weight and the free energy of each helical state, we can calculate the mole fraction f_P of monomer units taking the P helical state as a function of $\Delta G_{h,\alpha\beta}{}^\dagger$, and $\Delta G_{r,\alpha\beta}{}^\dagger$. It is noted that when $\Delta G_{r,\alpha\beta}{}^\dagger$ is large enough, high enantiomer excess $|2f_P - 1|$ is achieved even for a small $\Delta G_{h,\alpha\beta}{}^\dagger$ or at a little difference between $k_{P,\alpha\beta}$ and $k_{M,\alpha\beta}$.

We can also calculate f_P of block copolymers like poly-*b*-**2a$_n$3a$_m$** and poly-*b*-**4a$_n$5a$_m$** by applying the Ising model theory. In the block copolymers, the second block poly-**3a$_m$** or poly-**5a$_m$** is constructed by homopolymerization using the chiral initiator poly-**2a$_n$** or poly-**4a$_n$**. The probability a of the first reacting achiral monomer unit taking the P-state relative to that taking the M-state is given by

$$a = \frac{f_P k_{P,CA} + (1 - f_P)k_{r,CA}}{(1 - f_P)k_{M,CA} + f_P k_{r,CA}} \quad (2)$$

Because the second and succeeding reactions are just homopolymerization of achiral monomer, the enantiomer excess of the second block poly-**3a$_m$** should be determined by a and $\Delta G_{r,AA}{}^\dagger$. The method of calculating f_P for the dynamical helical chain polymerized by a chiral initiator is described in ref 15, and it can be applied to the nondynamical helical polyisocyanide chain by replacing the free energies by the activation free energies.

In the steady state of the chiral-achiral random copolymerization, the molar concentrations of the reacting chain ends [$\cdots$P] and [$\cdots$M] should be equal to the fractions f_P and $1 - f_P$ of the monomer units taking the P- and M-states, respectively, in the final polymer chain. Thus, the consumption rate $-$d[Mon]/dt of the total monomer (the chiral and achiral one) is given by

$$-\frac{d[Mon]}{dt} = \tilde{k}_{av}[I][Mon], \qquad \tilde{k}_{av} \equiv (\tilde{k}_P + \tilde{k}_r)f_P + (\tilde{k}_M + \tilde{k}_r)(1 - f_P) \quad (3)$$

where [I] (= [$\cdots$P] + [$\cdots$M]) is the molar concentration of the initiator, and $\tilde{k}_i$ (i = P, M, or r) is the average rate constant defined by

$$\tilde{k}_i = k_{i,CC}x^{*2} + 2k_{i,CA}x^*(1 - x^*) + k_{i,AA}(1 - x^*)^2 \quad (4)$$

with the mole fraction x^* of the C monomer in the total monomer in the reaction system. We here assume the perfectly random copolymerization, so that x^* is constant during the reaction.

Comparison with Experiment. To compare experimental results described in the Results section with the above-mentioned theory, we have to choose the maximum molar circular dichroism $\Delta\epsilon_{max}$ at 364 nm (or the maximum specific rotation) at $f_P = 1$, as well as the activation free energies, $\Delta G_{h,AC}{}^\dagger$, $\Delta G_{h,CA}{}^\dagger$, $\Delta G_{h,CC}{}^\dagger$, $\Delta G_{r,AA}{}^\dagger$, $\Delta G_{r,AC}{}^\dagger$, $\Delta G_{r,CA}{}^\dagger$, and $\Delta G_{r,CC}{}^\dagger$. In what follows, we assume that poly-**2a$_{100}$** and poly-**4a$_{100}$** are almost purely right-handed helical polymers, choosing $\Delta\epsilon_{max}$ = 13 dm^3 cm^{-3} mol^{-1} for poly-**2a$_{100}$** and 2.8 dm^3 cm^{-3} mol^{-1} for poly-**4a$_{100}$**. The ratio of $\Delta\epsilon_{364}$ to the average molar absorption coefficient ϵ at 364 nm is 7×10^{-3} for poly-**2a$_{100}$** and $3 \times$

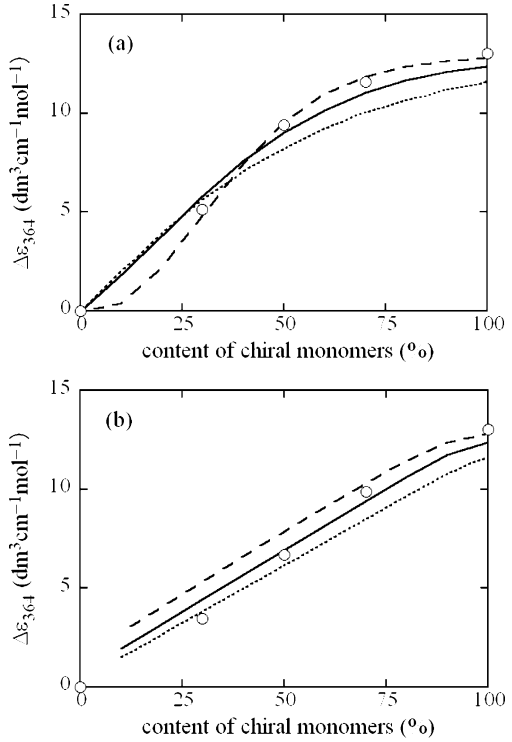

Figure 8. Comparison of the circular dichroism for (a) poly-*r*-**2a**$_n$**3a**$_m$ and (b) poly-*b*-**2a**$_n$**3a**$_m$ with the Ising model theory with the parameter sets ($\Delta G_{h,CA}^{\dagger}$, $\Delta G_{h,CC}^{\dagger}$, $\Delta G_r^{\dagger}$) = (−0.4, −0.95 or 0, 5) (dotted curve), (−0.15, −0.8 or 0, 7) (solid curve), and (0.02, −0.78 or 0, 9) (dashed curve) in units of kJ/mol.

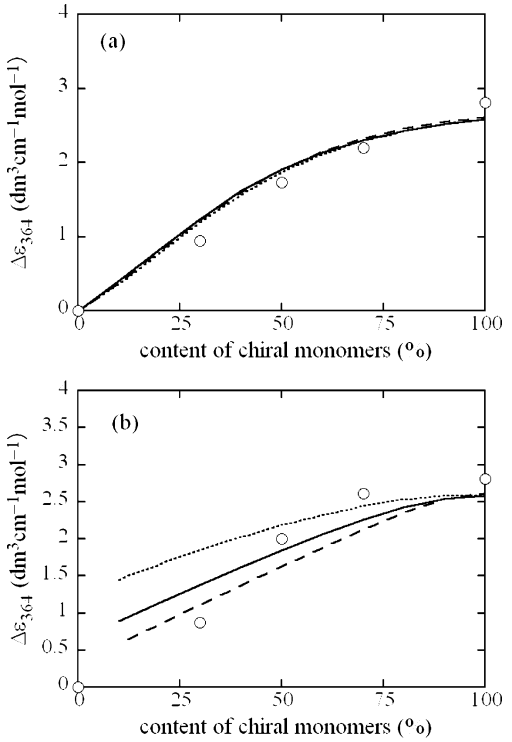

Figure 9. Comparison of the circular dichroism for (a) poly-*r*-**4a**$_n$**5a**$_m$ and (b) poly-*b*-**4a**$_n$**5a**$_m$ with the Ising model theory with the parameter sets ($\Delta G_{h,CA}^{\dagger}$, $\Delta G_{h,CC}^{\dagger}$, $\Delta G_r^{\dagger}$) = (−0.08, −0.35 or 0, 9) (dotted curve), (−0.05, −0.18 or 0, 11) (solid curve), and (−0.03, −0.11 or 0, 13) (dashed curve) in units of kJ/mol.

10^{-3} for poly-**4a$_{100}$**. These values are similar to or even larger than the ratio $\Delta\epsilon_{max}/\epsilon$ for optically active poly(aryl isocyanate)s ($\sim 3 \times 10^{-3}$), which may support the above assumption.

We first analyze the results of poly-*r*-**2a**$_n$**3a**$_m$ and poly-*b*-**2a**$_n$**3a**$_m$ shown in Figure 2. Since the chemical structures of **2a** and **3a** are similar, we may expect $\Delta G_{r,AA}^{\dagger} \approx \Delta G_{r,AC}^{\dagger} \approx \Delta G_{r,CC}^{\dagger}$ ($\equiv \Delta G_r^{\dagger}$) for their copolymers. Furthermore, to reduce the number of parameters, we assume that $\Delta G_{h,AC}^{\dagger} = \Delta G_{h,CA}^{\dagger}$. Then the enantiomer excess $2f_P - 1$ of poly-*r*-**2a**$_n$**3a**$_m$ should be determined by the three activation free energies, $\Delta G_{h,AC}^{\dagger}$, $\Delta G_{h,CC}^{\dagger}$, and $\Delta G_r^{\dagger}$. On the other hand, the calculation of $2f_P - 1$ of poly-*b*-**2a3a** does not need $\Delta G_{h,CC}^{\dagger}$ (see above).

As mentioned in the Results section, the ratio of the propagation rate constant $\tilde{k}_{av}$ of **2a** to that of **3a** was ca. 1.3. To make $\tilde{k}_{av}$ calculated by eq 3 agree with this experimental result, we have to choose a specific value of $\Delta G_{h,CC}^{\dagger}$ for a given $\Delta G_r^{\dagger}$ value. Figure 8 compares the theory and experiment of $\Delta\epsilon_{364}$ for poly-*r*-**2a**$_n$**3a**$_m$ and poly-*b*-**2a**$_n$**3a**$_m$ using three different $\Delta G_r^{\dagger}$. All three pairs of $\Delta G_{h,CC}^{\dagger}$ and $\Delta G_r^{\dagger}$ chosen in the figure provide the $\tilde{k}_{av}$ ratio of **2a** to **3a** to be 1.3. To reach to the experimental $\Delta\epsilon_{364}$ value of poly-**2a$_{100}$** at $x^* = 1$, we had to choose $\Delta G_r^{\dagger}$ larger than 5 kJ/mol. The value of $\Delta G_{h,CA}^{\dagger}$ was chosen so as to fit experimental $\Delta\epsilon_{364}$ of poly-*r*-**2a**$_n$**3a**$_m$. All three solid curves in Figure 8a succeed the fitting. The pairs of $\Delta G_{h,CA}^{\dagger}$ and $\Delta G_{h,CC}^{\dagger}$ chosen in panel a provide the three solid curves in panel b for $\Delta\epsilon_{364}$ of poly-*b*-**2a**$_n$**3a**$_m$. The best fit in this panel is achieved at $\Delta G_{h,CA}^{\dagger} = -800$ J/mol and $\Delta G_{h,CC}^{\dagger} = 7$ kJ/mol. The three curves in Panel b indicate that the $\Delta G_r^{\dagger}$ value is determined within 10−20% accuracy, and sensitivities of $\Delta\epsilon_{364}$ to $\Delta G_{h,CA}^{\dagger}$ and $\Delta G_{h,CC}^{\dagger}$ were in the same order.

Similar fittings were made for poly-*r*-**4a**$_n$**5a**$_m$ and poly-*b*-**4a**$_n$**5a**$_m$ shown in Figure 3. As shown in Figure 9, the best fit was obtained by choosing $\Delta G_{h,CA}^{\dagger} = -50$ J/mol, $\Delta G_{h,CC}^{\dagger} = -180$ J/mol, and $\Delta G_r^{\dagger} = 11$ kJ/mol. The more positive nonlinear relationship between $\Delta\epsilon_{364}$ and x^* for poly-*b*-**4a**$_n$**5a**$_m$ than poly-*b*-**2a**$_n$**3a**$_m$ comes mainly from the higher $\Delta G_r^{\dagger}$ value. These $\Delta G^{\dagger}$ parameters gives $\tilde{k}_{av}$ almost independent of x^*, which is consistent with narrow molecular weight distributions of poly-*r*-**4a**$_n$**5a**$_m$ samples.

Composition dependences of the circular dichroism for the other random copolyisocyanides were also compared with the Ising model theory. For poly-*r*-**2a**$_n$**5a**$_m$ and poly-*r*-**4a**$_n$**3a**$_m$, we should use the corresponding $\Delta G_{h,CC}^{\dagger}$, $\Delta G_{r,AA}^{\dagger}$, and $\Delta G_{r,CC}^{\dagger}$ determined above for poly-*r*-**2a**$_n$**3a**$_m$ and poly-*r*-**4a**$_n$**5a**$_m$. Only $\Delta G_{h,CA}^{\dagger}$ and $\Delta G_{r,CA}^{\dagger}$ are adjustable parameters to be newly determined. The enantiomer excess of poly-*r*-**2a**$_n$**4a**$_m$ synthesized from two chiral monomers can be also calculated by the Ising model theory using nonzero $\Delta G_{h,AA}^{\dagger}$. Here, $\Delta G_{h,AA}^{\dagger}$ should be equal to $\Delta G_{h,CC}^{\dagger}$ for poly-**4a$_{100}$**, and again $\Delta G_{h,CA}^{\dagger}$ and $\Delta G_{r,CA}^{\dagger}$ are the adjustable parameters. To calculate the circular dichroism of poly-*r*-**2a**$_n$**5a**$_m$, poly-*r*-**4a**$_n$**3a**$_m$, and poly-*r*-**2a**$_n$**4a**$_m$, we have assumed that the maximum circular dichroism changes with x^* by $\Delta\epsilon_{max} = \Delta\epsilon_{364}$(poly-**2a$_{100}$**)$x^* + \Delta\epsilon_{364}$(poly-**4a$_{100}$**)$(1 - x^*)$. Since the UV spectrum of poly-**6**$_m$ is similar to those of *m*-substitute poly(aryl isocyanide)s, we take $\Delta\epsilon_{364} = 2.8$ dm^3 cm^{-3} mol^{-1}. Furthermore, we assumed that $\Delta G_{r,AA}^{\dagger}$ and $\Delta G_{r,CA}^{\dagger}$ are equal to $\Delta G_{r,CC}^{\dagger}$ for poly-**4a$_{100}$** to fit the circular dichroism for poly-*r*-**4a**$_n$**6**$_m$ with adjusting the value of $\Delta G_{h,CA}^{\dagger}$. The fitting results are shown by solid, dotted, dot-dashed, and dashed curves in Figure 10, which are favorably compared with poly-*r*-**2a**$_n$**5a**$_m$, poly-*r*-**2a**$_n$**4a**$_m$, poly-*r*-**4a**$_n$**3a**$_m$, and poly-*r*-**4a**$_n$**6**$_m$, respectively. The negative nonlinearity in $\Delta\epsilon_{364}$ observed for poly-*r*-**2a**$_n$**5a**$_m$, poly-*r*-**2a**$_n$**4a**$_m$, and poly-*r*-**4a**$_n$**3a**$_m$ comes from positive $\Delta G_{h,CA}^{\dagger}$ opposite to negative $\Delta G_{h,CC}^{\dagger}$ (and $\Delta G_{h,AA}^{\dagger}$ in the case of poly-*r*-**2a**$_n$**4a**$_m$).

Table 7 lists average propagation rate constants $\tilde{k}_{av}$ of random copolymerizations for the aryl isocyanides investigated calculated by eq 3 using the activation free energies determined

Table 7. Average Propagation Rate Constants of the Random Copolymerization of Aryl Isocyanides Calculated by Eq 3

	$\tilde{k}_{av}/k_{AA}$					
*x**	poly-*r*-**2a**$_n$**3a**$_m$	poly-*r*-**4a**$_n$**5a**$_m$	poly-*r*-**2a**$_n$**5a**$_m$	poly-*r*-**2a**$_n$**4a**$_m$[a]	poly-*r*-**4a**$_n$**3a**$_m$	poly-*r*-**4a**$_n$**6**$_m$
0	1.08	1.02	1.02	1.08	1.08	1.02
0.2	1.09	1.02	1.17	1.18	1.22	1.03
0.5	1.16	1.04	1.30	1.29	1.28	1.06
0.8	1.29	1.06	1.35	1.31	1.18	1.07
1	1.40	1.08	1.40	1.40	1.08	1.08

[a] For poly-*r*-**2a**$_n$**4a**$_m$, *x** means the content of monomer **2a** in the two chiral monomer mixture.

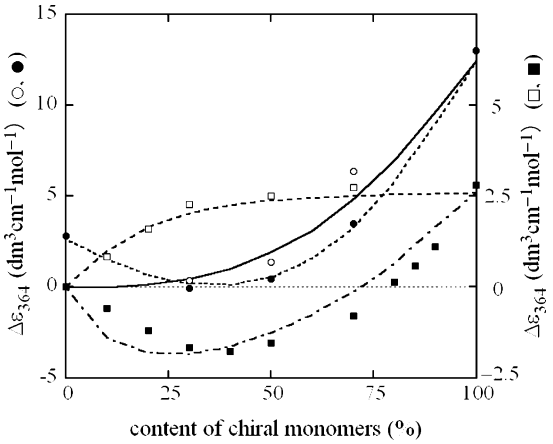

Figure 10. Comparison of the circular dichroism for poly-*r*-**2a**$_n$**5a**$_m$ (○), poly-*r*-**2a**$_n$**4a**$_m$ (●), poly-*r*-**4a**$_n$**3a**$_m$ (■), and poly-*r*-**4a**$_n$**6**$_m$ (□) with the Ising model theory with the parameter sets ($\Delta G_{h,AA}^{\dagger}$, $\Delta G_{h,CA}^{\dagger}$, $\Delta G_{h,CC}^{\dagger}$, $\Delta G_{r,AA}^{\dagger}$, $\Delta G_{r,CA}^{\dagger}$, $\Delta G_{r,CC}^{\dagger}$) = (0, 0.05, −0.8, 11, 2, 7) (solid curve), (−0.18, 0.5, −0.5, 11, 2, 7) (dotted curve), (0, 0.4, −0.18, 7, 2, 11) (dot-dashed curve), and (0, −0.15, −0.18, 11, 11, 11) (dashed curve) in units of kJ/mol.

above. The dependences of $\tilde{k}_{av}$ on *x** are weak for all copolymerizations, ensuring the random copolymerization and also narrow molecular weight distribution of the resulting copolymers. The dependences form a striking contrast to the strong *x** dependence of the enantiomer excess demonstrated by circular dichroism. Composition driven helical sense inversions like our poly-*r*-**4a**$_n$**3a**$_m$ were reported by Nolte et al. for a chiral-achiral copolymerization of isocyanides by a Ni catalysis. However, in their copolymerizations the propagation rate of the chiral monomer is much slower than that of the achiral monomer, and Nolte et al. interpreted the sense inversion by a slow propagation rate of the helix with the sense preferred by the chiral monomer: their chiral monomer acts as an inhibitor for the propagation reaction of one sense helix. Our mechanism of controlling the helical sense in random copolymers of chiral and achiral aryl isocyanides is completely different from their mechanism. Nolte et al.'s copolyisocyanides should possess large polydispersities in both molecular weight and composition, which are very much different from ours.

Summary

We have described the control of helical sense in random copolymers of aryl isocyanides possessing chiral and achiral alkoxycarbonyl groups at *p*- or *m*-positions. In these random copolymers, the helical structure of the main chain is determined by the helical sense selective polymerization, and the selectivity depends on the contents of chiral monomers and the structures of chiral and achiral monomers. These phenomena can be reasonably explained by the fact that the propagation reaction rate is determined cooperatively by the helical state and type of the active chain end monomer unit and also by the type of the reacting monomer. The preferential chirality of the pair of chiral and achiral monomers is sometimes opposite that of the pair of the same chiral monomers, leading to the composition driven helical sense inversion. Our findings are expected to be useful for the design of functional polyisocyanides with helical chirality.

Experimental Section

All reactions were carried out under argon atmosphere. THF was distilled over sodium benzophenone ketyl immediately before use. ^{13}C NMR spectra were measured with JEOL EX-270 and JNM-LA400 spectrometers in $CDCl_3$ using $SiMe_4$ as the internal standard. IR spectra were measured with a Perkin-Elmer system 2000 FT-IR, and gel permeation chromatography was performed with Shimadzu LC-6AD and SPD-10A using Shimadzu GPC-805, -804 and -8025 columns. THF was used as a mobile phase at a flow rate of 1.0 mL/min. The absolute molecular weights of poly-**2**$_n$ and poly-**4**$_n$, which were consistent with the calculated values based on the feed ratio of monomers and **1**, have been reported elsewhere.[9c] Specific rotation and CD spectra were measured with JASCO DIP-1000 and JASCO J-725, respectively. Elemental analyses were performed at the Material Analysis Center, ISIR, Osaka University. Pd−Pt μ-ethynediyl complex **1** and isocyanide monomers were prepared as reported previously.[9c,16]

Typical Procedure for Random Copolymerization. To a THF solution (20 mL) of *p*-(1*R*,2*S*,5*R*)-menthyloxycarbonylphenyl isocyanide (**2a**) (285 mg, 1.0 mmol) and *p*-cyclohexyloxycarbonylphenyl isocyanide (**3a**) (224 mg, 1.0 mmol) was added Pd−Pt μ-ethynediyl complex **1** (17 mg, 20 μmol), and the reaction mixture was stirred under reflux for 15 h. After the reaction mixture was concentrated to ca. 2 mL, the resulting solution was poured into methanol (100 mL). The precipitate was collected by filtration and washed with methanol several times to give yellow solid poly-*r*-**2a**$_{50}$**3a**$_{50}$ (495 mg, 93%). IR (cm^{-1}, KBr): 2090 ($\nu_{C\equiv C}$), 1715 ($\nu_{C=O}$), 1650 ($\nu_{C=N}$). ^{13}C NMR: δ 164.3 (C═O), 160.6 (C═N), 150.4 (Ar), 129.8 (Ar), 128.0 (Ar), 117.1 (Ar), 74.7 (menthyl−*C*H), 72.7 (Cy−*C*H), 47.2 (menthyl−*C*H), 41.0 (menthyl−*C*H$_2$), 34.3 (menthyl−*C*H$_2$), 31.5 (menthyl−*C*H), 31.5 (Cy−*C*H$_2$), 26.4 (menthyl−*C*H), 25.5 (Cy−*C*H$_2$), 23.6 (menthyl−*C*H$_2$), 22.0 (menthyl−*C*H$_3$), 20.7 (menthyl−*C*H$_3$), 16.5 (menthyl−*C*H$_3$). Anal. Calcd for $C_{1626}H_{1960}N_{100}Cl_2O_{200}P_4PdPt$: C, 73.41; H, 7.43; N, 5.27. Found: C, 73.49; H, 7.34; N, 5.32.

Typical Procedure for Block Copolymerization. A THF solution (20 mL) containing *p*-(1*R*,2*S*,5*R*)-menthyloxycarbonylphenyl isocyanide (**2a**) (228 mg, 0.80 mmol) and Pd−Pt μ-ethynediyl complex **1** (14 mg, 16 μmol) was refluxed for 15 h. After the complete consumption of **2a** was confirmed by GPC analysis, *p*-cyclohexyloxycarbonylphenyl isocyanide (**3a**) (183 mg, 0.80 mmol) was added. The reaction mixture was stirred for an additional 15 h, and was concentrated to ca. 2 mL. The resulting solution was poured into methanol (100 mL). The precipitate was filtered and washed with methanol to give yellow solid poly-*b*-**2a**$_{50}$**3a**$_{50}$ (383 mg, 90%). IR (cm^{-1}, KBr): 2090 ($\nu_{C\equiv C}$), 1715 ($\nu_{C=O}$), 1650 ($\nu_{C=N}$). ^{13}C NMR: δ 164.3 (C═O), 162.1 (C═N), 160.6 (C═N), 150.4 (Ar), 129.6 (Ar), 127.8 (Ar), 117.6 (Ar), 74.7 (menthyl−*C*H), 72.7 (Cy−*C*H), 47.3 (menthyl−*C*H), 41.1 (menthyl−*C*H$_2$), 34.4 (menthyl−*C*H$_2$), 31.4 (menthyl−*C*H), 31.4 (Cy−*C*H$_2$), 26.4 (menthyl−*C*H), 25.6 (Cy−*C*H$_2$), 23.7 (menthyl−*C*H$_2$), 22.0 (menthyl−*C*H$_3$), 20.7 (menthyl−*C*H$_3$), 16.5 (br, menthyl−*C*H$_3$). Anal. Calcd for $C_{1626}H_{1960}N_{100}Cl_2O_{200}P_4PdPt$: C, 73.41; H, 7.43; N, 5.27. Found: C, 73.61; H, 7.24; N, 5.36.

Random Copolymer Poly-*r*-2a$_{50}$3b$_{50}$. This was obtained as a yellow solid in 87% yield. IR (cm^{-1}, KBr): 2091 ($\nu_{C\equiv C}$), 1715 ($\nu_{C=O}$), 1650 ($\nu_{C=N}$). ^{13}C NMR: δ 164.8 (C═O), 161.8 (C═N), 150.6 (Ar), 129.8 (Ar), 127.8 (Ar), 117.1 (Ar), 74.7 (menthyl−*C*H), 66.2 (Pr−*C*H$_2$), 47.1 (menthyl−*C*H), 40.7 (menthyl−*C*H$_2$), 34.3 (menthyl−*C*H$_2$), 31.6 (menthyl−*C*H), 26.5 (menthyl−*C*H), 23.9 (menthyl−*C*H$_2$), 22.0 (menthyl−*C*H$_2$), 22.0 (Pr−*C*H$_2$), 20.7 (menthyl−*C*H$_3$), 16.5 (menthyl−*C*H$_3$), 10.3 (Pr−*C*H$_3$). Anal. Calcd for $C_{1476}H_{1810}N_{100}Cl_2O_{200}P_4PdPt$: C, 71.92; H, 7.40; N, 5.68. Found: C, 72.17; H, 7.22; N, 5.73.

Block Copolymer Poly-*b*-2a$_{50}$3b$_{50}$. This was obtained as a yellow solid in 88% yield. IR (cm^{-1}, KBr): 2088 ($\nu_{C\equiv C}$), 1715 ($\nu_{C=O}$), 1650 ($\nu_{C=N}$). ^{13}C NMR: δ 164.9 (C═O), 160.8 (C═N), 150.4 (Ar), 129.7 (Ar), 127.2 (Ar), 118.4 (Ar), 74.7 (menthyl−*C*H), 66.2 (Pr−*C*H$_2$), 47.1 (menthyl−*C*H), 40.7 (menthyl−*C*H$_2$), 34.3 (menthyl−*C*H$_2$), 31.6 (menthyl−*C*H), 26.5 (menthyl−*C*H), 23.8 (menthyl−*C*H$_2$), 21.8 (menthyl−*C*H$_3$), 21.8 (Pr−*C*H$_2$), 20.7 (menthyl−*C*H$_3$), 16.5 (menthyl−*C*H$_3$), 10.3 (Pr−*C*H$_3$). Anal. Calcd for $C_{1476}H_{1810}N_{100}Cl_2O_{200}P_4PdPt$: C, 71.92; H, 7.40; N, 5.68. Found: C, 72.19; H, 7.19; N, 5.88.

Random Copolymer Poly-*r*-4a$_{50}$5a$_{50}$. This was obtained as a yellow solid in 83% yield. IR (cm^{-1}, KBr): 2090 ($\nu_{C\equiv C}$), 1715 ($\nu_{C=O}$), 1650 ($\nu_{C=N}$). ^{13}C NMR: δ 164.4 (C═O), 162.7 (C═N), 147.4 (Ar), 130.2 (Ar), 127.9 (Ar), 125.8 (Ar), 119.1 (Ar), 117.1 (Ar), 74.0 (menthyl−*C*H), 72.9 (Cy−*C*H), 47.0 (menthyl−*C*H), 40.7 (menthyl−*C*H$_2$), 34.3 (menthyl−*C*H$_2$), 31.6 (menthyl−*C*H), 31.6 (Cy−*C*H$_2$), 26.3 (menthyl−*C*H), 25.5 (Cy−*C*H$_2$), 23.7 (menthyl−*C*H$_2$), 22.1 (menthyl−*C*H$_3$), 20.9 (menthyl−*C*H$_3$), 16.4 (menthyl−*C*H$_3$). Anal. Calcd for $C_{1626}H_{1960}N_{100}Cl_2O_{200}P_4PdPt$: C, 73.41; H, 7.43; N, 5.27. Found: C, 73.61; H, 7.27; N, 5.14.

Block Copolymer Poly-*b*-4a$_{50}$5a$_{50}$. This was obtained as a yellow solid in 85% yield. IR (cm^{-1}, KBr): 2088 ($\nu_{C\equiv C}$), 1715 ($\nu_{C=O}$), 1650 ($\nu_{C=N}$). ^{13}C NMR: δ 164.5 (C═O), 162.9 (C═N), 161.5 (C═N), 147.4 (Ar), 130.2 (Ar), 127.7 (Ar), 125.8 (Ar), 121.7 (Ar), 119.1 (Ar), 74.7 (menthyl−*C*H), 72.7 (Cy−*C*H), 47.3 (menthyl−*C*H), 41.1 (menthyl−*C*H$_2$), 34.4 (menthyl−*C*H$_2$), 31.4 (menthyl−*C*H), 31.4 (Cy−*C*H$_2$), 26.4 (menthyl−*C*H), 25.6 (Cy−*C*H$_2$), 23.7 (menthyl−*C*H$_2$), 22.0 (menthyl−*C*H$_3$), 20.7 (menthyl−*C*H$_3$), 16.5 (menthyl−*C*H$_3$). Anal. Calcd for $C_{1626}H_{1960}N_{100}Cl_2O_{200}P_4$-PdPt: C, 73.41; H, 7.43; N, 5.27. Found: C, 73.61; H, 7.11; N, 5.24.

Random Copolymer Poly-*r*-4a$_{50}$5b$_{50}$. This was obtained as a yellow solid in 87% yield. IR (cm^{-1}, KBr): 2091 ($\nu_{C\equiv C}$), 1715 ($\nu_{C=O}$), 1650 ($\nu_{C=N}$). ^{13}C NMR: δ 164.7 (C═O), 162.9 (C═N), 161.3 (C═N), 147.3 (Ar), 129.9 (Ar), 127.7 (Ar), 125.8 (Ar), 121.6 (Ar), 119.1 (Ar), 74.5 (menthyl−*C*H), 66.2 (Pr−*C*H$_2$), 47.2 (menthyl−*C*H), 40.9 (menthyl−*C*H$_2$), 34.2 (menthyl−*C*H$_2$), 31.4 (menthyl−*C*H), 26.3 (menthyl−*C*H), 23.5 (menthyl−*C*H$_3$), 22.0 (menthyl−*C*H$_3$), 22.0 (Pr−*C*H$_2$), 20.7 (menthyl−*C*H$_3$), 16.4 (menthyl−*C*H$_3$), 10.3 (Pr−*C*H$_3$). Anal. Calcd for $C_{1476}H_{1810}N_{100}Cl_2O_{200}P_4$-PdPt: C, 71.92; H, 7.40; N, 5.68. Found: C, 71.65; H, 7.16; N, 5.73.

Block Copolymer Poly-*b*-4a$_{50}$5b$_{50}$. This was obtained as a yellow solid in 89% yield. IR (cm^{-1}, KBr): 2090 ($\nu_{C\equiv C}$), 1715 ($\nu_{C=O}$), 1650 ($\nu_{C=N}$). ^{13}C NMR: δ 164.7 (C═O), 163.7 (C═N), 160.6 (C═N), 147.4 (Ar), 129.7 (Ar), 127.8 (Ar), 125.8 (Ar), 122.0 (Ar), 118.9 (Ar), 73.9 (menthyl−*C*H), 65.9 (Pr−*C*H$_2$), 47.1 (menthyl−*C*H), 40.7 (menthyl−*C*H$_2$), 34.4 (menthyl−*C*H$_2$), 31.4 (menthyl−*C*H), 31.4 (Cy−*C*H$_2$), 26.3 (menthyl−*C*H), 23.7 (menthyl−*C*H$_2$), 22.0 (menthyl−*C*H$_3$), 21.8 (Pr−*C*H$_2$), 20.8 (menthyl−*C*H$_3$), 16.4 (menthyl−*C*H$_3$), 10.3 (Pr−*C*H$_3$). Anal. Calcd for $C_{1476}H_{1810}N_{100}Cl_2O_{200}P_4PdPt$: C, 71.92; H, 7.40; N, 5.68. Found: C, 71.72; H, 7.28; N, 5.42.

Random Copolymer Poly-*r*-4a$_{50}$6$_{50}$. This was obtained as a yellow solid in 87% yield. IR (cm^{-1}, KBr): 2088 ($\nu_{C\equiv C}$), 1715 ($\nu_{C=O}$), 1650 ($\nu_{C=N}$). ^{13}C NMR: δ 163.3 (C═O), 161.5 (C═N), 147.2 (Ar), 130.3 (Ar), 127.8 (Ar), 125.1 (Ar), 121.1 (Ar), 119.3 (Ar), 74.0 (menthyl−*C*H), 66.0 (Pr−*C*H$_2$), 47.0 (menthyl−*C*H), 40.9 (menthyl−*C*H$_2$), 34.4 (menthyl−*C*H$_2$), 31.6 (menthyl−*C*H), 25.9 (menthyl−*C*H), 23.1 (menthyl−*C*H$_2$), 21.9 (menthyl−*C*H$_3$), 21.9 (Pr−*C*H$_2$), 21.2 (menthyl−*C*H$_3$), 16.2 (menthyl−*C*H$_3$), 10.2 (Pr−*C*H$_3$). Anal. Calcd for $C_{1676}H_{2060}N_{100}Cl_2O_{200}P_4PdPt$: C, 69.65; H, 7.18; N, 4.85. Found: C, 69.90; H, 6.90; N, 4.77.

Random Copolymer Poly-*r*-2a$_{50}$5a$_{50}$. This was obtained as a yellow solid in 87% yield. IR (cm^{-1}, KBr): 2088 ($\nu_{C\equiv C}$), 1715 ($\nu_{C=O}$), 1650 ($\nu_{C=N}$). ^{13}C NMR: δ 164.3 (C═O), 161.2 (C═N), 150.6 (Ar), 147.4 (Ar), 129.9 (Ar), 127.5 (Ar), 116.8 (Ar), 74.4 (menthyl−*C*H), 72.8 (Cy−*C*H), 47.2 (menthyl−*C*H), 41.0 (menthyl−*C*H$_2$), 34.3 (menthyl−*C*H$_2$), 31.4 (menthyl−*C*H), 31.4 (Cy−*C*H$_2$), 26.4 (menthyl−*C*H), 25.4 (Cy−*C*H$_2$), 23.7 (menthyl−*C*H$_2$), 22.0 (menthyl−*C*H$_3$), 20.7 (menthyl−*C*H$_3$), 16.5 (menthyl−*C*H$_3$). Anal. Calcd for $C_{1626}H_{1960}N_{100}Cl_2O_{200}P_4PdPt$: C, 73.41; H, 7.43; N, 5.27. Found: C, 73.18; H, 7.22; N, 5.27.

Random Copolymer Poly-*r*-4a$_{50}$3a$_{50}$. This was obtained as a yellow solid in 78% yield. IR (cm^{-1}, KBr): 2088 ($\nu_{C\equiv C}$), 1715 ($\nu_{C=O}$), 1650 ($\nu_{C=N}$). ^{13}C NMR: δ 164.3 (C═O), 162.5 (C═N), 150.5 (Ar), 147.5 (Ar), 129.5 (Ar), 127.6 (Ar), 125.9 (Ar), 117.1 (Ar), 74.6 (menthyl−*C*H), 72.6 (Cy−*C*H), 47.2 (menthyl−*C*H), 40.9 (menthyl−*C*H$_2$), 34.3 (menthyl−*C*H$_2$), 31.5 (menthyl−*C*H), 31.5 (Cy−*C*H$_2$), 26.4 (menthyl−*C*H), 25.5 (Cy−*C*H$_2$), 23.6 (menthyl−*C*H$_2$), 22.0 (menthyl−*C*H$_3$), 20.8 (menthyl−*C*H$_3$), 16.4 (menthyl−*C*H$_3$). Anal. Calcd for $C_{1626}H_{1960}N_{100}Cl_2O_{200}P_4PdPt$: C, 73.41; H, 7.43; N, 5.27. Found: C, 73.61; H, 7.23; N, 5.07.

Random Copolymer Poly-*r*-2a$_{50}$4a$_{50}$. This was obtained as a yellow solid in 91% yield. IR (cm^{-1}, KBr): 2087 ($\nu_{C\equiv C}$), 1715 ($\nu_{C=O}$), 1651 ($\nu_{C=N}$). ^{13}C NMR: δ 164.3 (C═O), 161.6 (C═N), 150.8 (Ar), 147.4 (Ar), 129.9 (Ar), 127.6 (Ar), 125.7 (Ar), 121.0 (Ar), 119.1 (Ar), 74.0 (menthyl−*C*H), 47.2 (menthyl−*C*H), 40.9 (menthyl−*C*H$_2$), 34.3 (menthyl−*C*H$_2$), 31.4 (menthyl−*C*H), 26.4 (menthyl−*C*H), 23.5 (menthyl−*C*H$_2$), 22.0 (menthyl−*C*H$_3$), 20.8 (menthyl−*C*H$_3$), 16.4 (menthyl−*C*H$_3$). Anal. Calcd for $C_{1826}H_{2360}N_{100}$-$Cl_2O_{200}P_4PdPt$: C, 74.58; H, 8.09; N, 4.76. Found: C, 74.36; H, 8.12; N, 4.69.

Acknowledgment. This work was partly supported by a Grant-in-Aid for Scientific Research in a Priority Area "Super-Hierarchical Structures (No. 446)", a Grant-in-Aid for Scientific Research (No. 17350058), and also Special Coordination Funds for Promoting Science and Technology ("Yuragi Project") of the Ministry of Education, Culture, Sports, Science and Technology, Japan. We thank the members of the Materials Analysis Center, ISIR, Osaka University, for spectral measurements and microanalyses.

References and Notes

(1) For recent reviews, see: (a) Hill, D. J.; Mio, M. J.; Prince, R. B.; Hughes, T. S.; Moore, J. S. *Chem. Rev.* **2001**, *101*, 3893. (b) Nakano, T.; Okamoto, Y. *Chem. Rev.* **2001**, *101*, 4013. (c) Cornelissen, J. J. L. M.; Rowan, A. E.; Nolte, R. J. M.; Sommerdijk, N. A. J. M. *Chem. Rev.* **2001**, *101*, 4039. (d) Green, M. M.; Cheon, K.-S.; Yang, S.-Y.; Park, J.-W.; Swansburg, S.; Liu, W. *Acc. Chem. Res.* **2001**, *34*, 672. (e) Yashima, E.; Maeda, K.; Nishimura, T. *Chem.—Eur. J.* **2004**, *10*, 42.

(2) (a) Green, M. M.; Reidy, M. P.; Johnson, R. D.; Darling, G.; O'Leary, D. J.; Willson, G. *J. Am. Chem. Soc.* **1989**, *111*, 6452. (b) Lifson, S.; Green, M. M.; Andreola, C.; Peterson, N. C. *J. Am. Chem. Soc.* **1989**, *111*, 8850. (c) Gu, H.; Nakamura, Y.; Sato, T.; Teramoto, A.; Green, M. M.; Jha, S. K.; Andreola, C.; Reidy, M. P. *Macromolecules* **1998**, *31*, 6362.

(3) (a) Yashima, E.; Huang, S.; Matsushima, T.; Okamoto, Y. *Macromolecules* **1995**, *28*, 4184. (b) Nomura, R.; Fukushima, Y.; Nakako, H.; Masuda, T. *J. Am. Chem. Soc.* **2000**, *122*, 8830. (c) Maeda, K.; Morino, K.; Okamoto, Y.; Sato, T.; Yashima, E. *J. Am. Chem. Soc.* **2004**, *126*, 4329.

(4) For reviews, see: (a) Green, M. M.; Peterson, N. C.; Sato, T.; Teramoto, A.; Cook, R.; Lifson, S. *Science* **1995**, *268*, 1860. (b) Green, M. M.; Park, J.-W.; Sato, T.; Teramoto, A.; Lifson, S.; Selinger, R. L. B.; Selinger, J. V. *Angew. Chem., Int. Ed.* **1999**, *38*, 3139. (c) Sato, T.; Terao, K.; Teramoto, A.; Fujiki, M. *Polymer* **2003**, *44*, 5477.

(5) For reviews, see: (a) Millich, F. *Chem. Rev.* **1972**, *72*, 101. (b) Drenth, W.; Nolte, R. J. M. *Acc. Chem. Res.* **1979**, *12*, 30. (c) Nolte, R. J. M. *Chem. Soc. Rev.* **1994**, *23*, 11. (d) Suginome, M.; Ito, Y. *Adv. Polym. Sci.* **2004**, *171*, 77.

(6) Nolte, R. J. M.; van Beijnen, A. J. M.; Drenth, W. *J. Am. Chem. Soc.* **1974**, *96*, 5932.

(7) Kamer, P. C. J.; Cleij, M. C.; Nolte, R. J. M.; Harada, T.; Hezemans, A. M. F.; Drenth, W. *J. Am. Chem. Soc.* **1988**, *110*, 1581.
(8) (a) Onitsuka, K.; Joh, T.; Takahashi, S. *Angew. Chem., Int. Ed. Engl.* **1992**, *31*, 851. (b) Onitsuka, K.; Yanai, K.; Takei, F.; Joh, T.; Takahashi, S. *Organometallics* **1994**, *13*, 3862.
(9) (a) Takei, F.; Yanai, K.; Onitsuka, K.; Takahashi, S. *Angew. Chem., Int. Ed. Engl.* **1996**, *35*, 1554. (b) Takei, F.; Onitsuka, K.; Takahashi, S. *Polym. J.* **1999**, *31*, 1029. (c) Takei, F.; Yanai, K.; Onitsuka, K.; Takahashi, S. *Chem.—Eur. J.* **2000**, *6*, 983. (d) Takei, F.; Hayashi, H.; Onitsuka, K.; Takahashi, S. *Polym. J.* **2001**, *33*, 310. (e) Takei, F.; Hayashi, H.; Onitsuka, K.; Kobayashi, N.; Takahashi, S. *Angew. Chem., Int. Ed.* **2001**, *40*, 4092. (f) Hida, N.; Takei, F.; Onitsuka, K.; Shiga, K.; Asaoka, S.; Iyoda, T.; Takahashi, S. *Angew. Chem., Int. Ed.* **2003**, *42*, 4349.
(10) Takei, F.; Onitsuka, K.; Takahashi, S. *Polym. J.* **2000**, *32*, 524.
(11) Koe, J. R.; Fujiki, M.; Motonaga, M.; Nakashima, H. *Macromolecules* **2001**, *34*, 1082.
(12) Sato, T.; Terao, K.; Teramoto, A.; Fujiki, M. *Macromolecules* **2002**, *35*, 5355.
(13) (a) Deng, J.; Tabei, J.; Shiotsuki, M.; Sanda, F.; Masuda, T. *Macromolecules* **2004**, *37*, 9715. (b) Tabei, J.; Shiotsuki, M.; Sato, T.; Sanda, F.; Masuda, T. *Chem.—Eur. J.* **2005**, *11*, 3591.
(14) Maeda, K.; Okamoto, Y. *Macromolecules* **1999**, *32*, 974.
(15) Gu, H.; Sato, T.; Teramoto, A.; Varichon, L.; Green, M. M. *Polym. J.* **1997**, *29*, 77.
(16) Onitsuka, K.; Joh, T.; Takahashi, S. *Bull. Chem. Soc. Jpn.* **1992**, *65*, 1179.

MA070891W